NMR studies of molecular ordering and molecular dynamics in a chiral liquid crystal with the SmC_α^* phase

Magdalena Knapkiewicz [1], Adam Rachocki [1,*], Michał Bielejewski [1], and Pedro J. Sebastião [2,3]

[1] *Institute of Molecular Physics, Polish Academy of Sciences, M. Smoluchowskiego 17, 60-179 Poznan, Poland*

[2] *Center of Physics and Engineering of Advanced Materials, Instituto Superior Técnico, Universidade de Lisboa, Av. Rovisco Pais, 1049-001 Lisbon, Portugal*

[3] *Department of Physics, Instituto Superior Técnico, Universidade de Lisboa, Av. Rovisco Pais, 1049-001 Lisbon, Portugal*

(Received 3 February 2020; accepted 30 April 2020; published 28 May 2020)

Molecular dynamics of the antiferroelectric liquid crystal 4′-(octyloxy)biphenyl-4-carboxylate2-fluoro-4-[(octyl-2-yloxy)carbonyl]phenyl (abbreviated as D16) was investigated using different nuclear magnetic resonance (NMR) techniques. D16 molecules form a smectic-C_α^* phase (SmC_α^*) in an extremely wide temperature range (∼10 °C). Due to a small tilt of the molecules, this phase is characterized by short switching times, important for new photonic applications. The proton spin-lattice relaxation times were measured in isotropic (Iso), smectic-*A* (Sm*A*), and SmC_α^* phases over a wide frequency range of five decades, with conventional and fast field-cycling NMR techniques. This approach allowed a comparison of the essential processes of molecular dynamics taking place in these phases. On the basis of NMR relaxometry measurements, we present a description of the motional behavior of liquid crystal molecules forming SmC_α^*. Pretransitional effects were observed in wide temperature ranges in both the isotropic and Sm*A* phases in D16. The ^{1}H fast field-cycling NMR measurements were supplemented with NMR diffusometry and ^{19}F NMR spectroscopy.

DOI: 10.1103/PhysRevE.101.052708

I. INTRODUCTION

Liquid crystals (LCs) were discovered at the end of the 19th century and are still an interesting subject of research for scientists and engineers. Through the years, more and more compounds with liquid crystalline properties have been synthesized, including those exhibiting LC phases showing complex and sometimes exotic orientational and positional orders over short- and long-range distances. At the end of the 20th century the property of ferroelectricity in LCs was discovered, and more than a decade later the property of antiferroelectricity was finally identified. These discoveries have aroused great interest from industry because of very promising electrical and optical properties of ferroelectric liquid crystals (FLCs) and antiferroelectric liquid crystals (AFLCs), which are crucial in particular for high-resolution displays [1].

This paper reports the studies of local and collective molecular dynamics in a thermotropic LC with rodlike molecules ("calamitic"). This type of LCs form mesophases generally classified in two categories: one-dimensionally ordered nematics (N) and two-dimensionally ordered smectics (Sm) [2–4]. In this article only smectic phases with liquidlike layers are considered. Taking into account the molecular order in layers, its several types can be distinguished. The smectic-*A* phase (Sm*A*) molecules in the layers are oriented, on average, in parallel to the layer normal, whereas in all types of smectic-*C* phases (Sm*C*) molecules are tilted at an angle to the layer normal.

In liquidlike tilted smectics composed of chiral molecules with transverse electric dipole moments (e.g., in SmC^*), each molecular layer exhibits nonzero spontaneous polarization. The direction of spontaneous polarization vectors can be modified using an external electric field. The macroscopic polarization dependence on an electric field is specific to every chiral smectic phase [5]. Such smectics between polymer-coated glass substrates at a distance of a few micrometers exhibit ferro-, ferri-, or antiferroelectricity [6,7].

The antiferroelectric liquid crystals (AFLCs) are attractive to industry because of their unique properties, including tristate electrical switching behavior, easy dc compensation, electrooptical response on the order of microseconds, hemispherical viewing angle, intrinsic analog gray-scale capability, and absence of a ghost effect [8]. However, the display devices based on AFLCs are still in the development stage, and more studies are required to allow a full market expansion. Moreover, AFLCs are also important from the point of view of basic studies, as AFLC materials show various subphases of different molecular ordering exhibiting different effects like second-order transitions.

It is well known that the anisotropic optical properties of LCs can be used to achieve electro-optical response by controlling the alignment of the LC molecules along the applied external electric field [2,4]. It is also known that the electro-optical response in chiral smectics could be several orders of magnitude faster than in nematics [7,9]. In FLCs the response is in the range of tens of milliseconds [10], whereas in AFLCs it is shorter and can be in the range of

*adam.rachocki@ifmpan.poznan.pl

single milliseconds [10] or even a few microseconds [11]. Nowadays, an enormous effort is being undertaken to find materials that are characterized by the fast molecular response under a low electric field applied. Such materials are suitable for numerous applications in industry due to specific electrooptical properties. The AFLCs are materials which could achieve this goal if some basic problems and limitations are overcome.

One possible material candidate is a LC with a smectic-C_α^* phase (SmC_α^*). In this intriguing phase, the molecules are tilted at a small constant angle (e.g., 10°) between the layer normal and the tilt direction. The tilt direction changes from layer to layer and molecules form helical superstructure similarly as in SmC^* [12]. However, the helix formed by the tilted molecules in SmC^* phase can be composed of around several hundred layers, whereas in SmC_α^* phase the helix can be formed by only a few layers. Moreover, in SmC_α^* the tilt angle is smaller than in SmC^* (e.g., 30°). This allows a faster response to the applied electric field. The largest limitation in the use of SmC_α^* phase is related to its rather narrow temperature range, typically a few degrees centigrade.

Although many papers dealing with electrooptical properties of the SmC_α^* phase have been published, no results have been reported as yet to the best of our knowledge concerning the study of molecular dynamics using nuclear magnetic resonance (NMR) techniques [13–15]. Recently a substantial broadening of the temperature range of the SmC_α^* phase occurrence has become within reach. Two flagship examples of such a broadening of the temperature range of the SmC_α^* phase are (1) the use of chiral dopants that widen the phase existence range from around 2 to 21 °C and (2) polymer network creation to widen the phase existence range from 3 to 39 °C [16,17]. Mesogen, nicknamed D16, exhibits SmC_α^* in a very broad temperature range, approximately 10 °C [13]. This material is potentially attractive for applications and can be treated as a good candidate for further temperature stabilization of SmC_α^* phase (for instance, by photopolymerization of a suitable polymer precursor).

Here we present molecular dynamic studies of D16 by means of fast field cycling ^{1}H NMR relaxometry (FFC NMR). The FFC NMR technique makes it possible to obtain detail information about both individual and collective molecular motions in different LC phases [18–21].

In addition, the ^{19}F NMR spectra were obtained to follow the phase transitions to establish the orientational order parameters as well as tilt angles in smectic phases detected in D16. Moreover, both ^{19}F NMR spectroscopy and ^{19}F NMR diffusometry allowed determination of SmA clusters in the isotropic phase. It is worth notingthat there is only one fluorine atom per 87 atoms included in the D16 molecule. All this has convinced us that NMR is a powerful tool to characterize LC systems [22].

II. MATERIAL AND METHODS

The antiferroelectric LC 4′-(octyloxy)biphenyl-4-carboxylate-2-fluoro-4-[(octyl2yloxy)carbonyl]phenyl, abbreviated as D16, was purchased from the AWAT Company (Warsaw, Poland). The structural formula of this mesogen is depicted in Fig. 1.

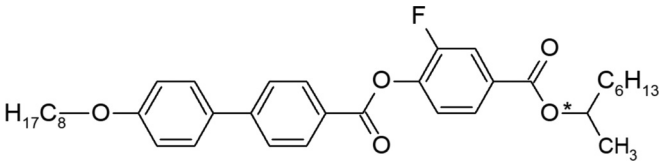

FIG. 1. The structural formula of the D16 mesogen; diameter of the molecule $d = 5$ Å and length $l = 35$ Å.

The phase sequence on cooling D16 from the isotropic (Iso) phase is

$$\mathrm{Cr} \overset{38\,^\circ\mathrm{C}}{\leftarrow} \mathrm{SmC}_\beta^* \overset{50\,^\circ\mathrm{C}}{\leftarrow} \mathrm{SmC}_\alpha^* \overset{60\,^\circ\mathrm{C}}{\leftarrow} \mathrm{SmA} \overset{119\,^\circ\mathrm{C}}{\leftarrow} \mathrm{Iso}.$$

The temperatures of the phase transitions between smectic phases were determined using dielectric spectroscopy [15], whereas the temperature of the isotropic/LC phase transition as well as crystallization temperature were verified using differential scanning calorimetry (see the Supplemental Material [23] Fig. S1). The presence of the SmC_α^* phase was also confirmed with the reversal current method (RCM) applying the triangular electric field [15].

The NMR diffusion measurements and the ^{19}F NMR spectroscopic experiments were performed with a Bruker Avance III HD spectrometer coupled to a superconducting vertical wide-bore (89-mm) Ascend magnet operating at 11.74 T (500 MHz for ^{1}H). The NMR spectra were collected as a function of temperature, T, every 2 °C, on cooling from the isotropic (135 °C) to the crystalline (22 °C) phase. Moreover, this system is equipped with a gradient unit and a diffusion probe for ^{1}H and ^{19}F NMR diffusion experiments. The maximum gradient strength in the z direction is of 30 Tm^{-1}. The pulse gradient stimulated echo sequence (PGSTE) was used to measure the diffusion coefficient of LC molecules in the isotropic phase.

The sample was placed inside a diffusion probe in a 5-mm-diameter glass tube. The measurements were performed on ^{19}F isotopes in the isotropic phase of D16. The methodology of this experiment has been described in detail in our previous work [24]. The self-diffusion coefficients D determined in this way were then used as fixed model parameters in the analysis of the NMR dispersion (NMRD) profiles.

The NMRD profiles represent the proton spin-lattice relaxation rates ($1/T_1$) recorded as a function of magnetic field strength from 0.235 mT to 0.450 T (covering the ^{1}H Larmor frequencies, ν_L, from 10 kHz to 20 MHz) using a SpinMaster 2000 Fast Field Cycling (FFC) relaxometer (Stelar, Mede, Italy). The details of this experimental technique are reported elsewhere, and here only the basic concept is provided [25–27]. In the FFC T_1 measurement method, the magnetic field is changed by switching the current in a solenoid magnet. The time evolution of magnetization is observed at a given yet adjustable magnetic field called the relaxation field (B_{relax}), for a variable period of time, which allows determination of T_1 and thus studies of the molecular dynamics in the material under investigation. At the end of the evolution time, the magnetic field is switched to an acquisition field (B_{acq}) at which the longitudinal magnetization is detected after applying a $\pi/2$ RF pulse to obtain the free induction decay (FID).

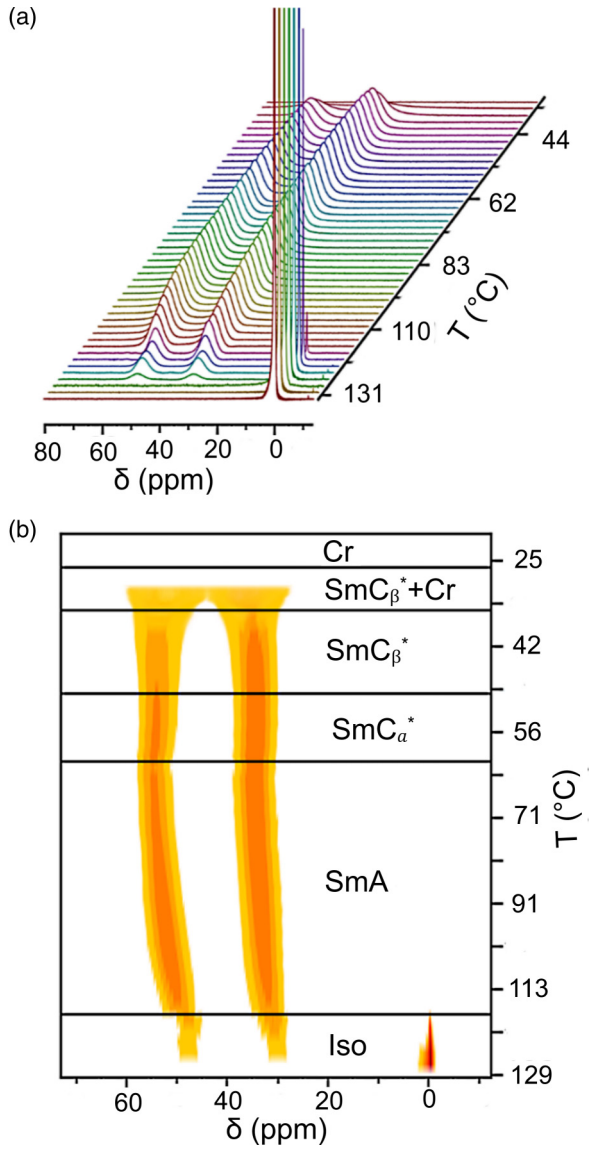

FIG. 2. The ^{19}F NMR spectra (a) and the gradient map of the signal intensity (b) in D16 presented as a function of temperature; $\delta-$ chemical shift.

The relaxation profiles for D16 were recorded at 10 temperatures on cooling from the isotropic phase: 135, 125 °C (within the Iso phase), 115, 95, 75, 65 °C (within the Sm*A* phase), and 60, 58, 55, 52 °C (within the Sm$C_\alpha{}^*$ phase). Additional experimental points in the relaxation profiles were obtained with the inversion recovery sequence at Larmor frequencies of 43.4, 90, and 500 MHz using the appropriate variable field (0–2 T) electromagnet Bruker BE30 with AVANCE II console and Bruker Avance III HD spectrometer equipped with an Ascend magnet (11.7 T).

III. RESULTS AND DISCUSSION

A. ^{19}F NMR spectroscopy

The ^{19}F NMR spectra recorded as a function of temperature in various mesophases of D16 LC are presented in Fig. 2. In the isotropic phase for temperatures above 131 °C only one narrow line is detected. It can be explained by fast dynamics of molecules leading to averaging of dipole-dipole interactions. At the temperatures close to the Sm*A* phase transition temperature, the strong isotropic peak starts to disappear, and a characteristic doublet starts to appear and shifts towards higher chemical shift values as a consequence of the transition from isotropic phase to Sm*A* phase. The doublet observed in the range from 60 to 30 ppm is caused by dipolar splitting of the spin pairs composed of fluorine and proton belonging to the benzene rings of D16 (see Fig. 1)

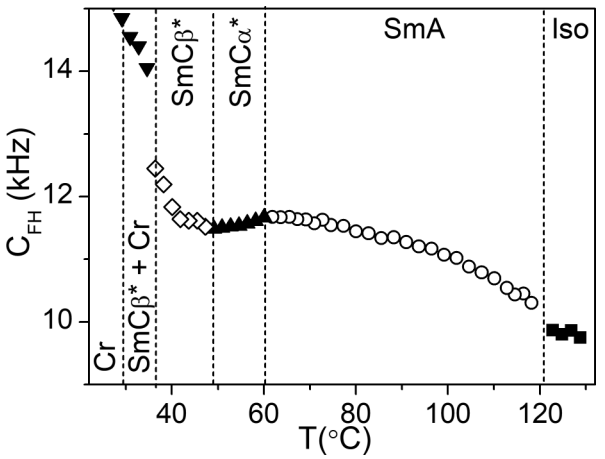

FIG. 3. The temperature dependence of the change in spin-spin coupling constant, C_{FH}.

Close to the Iso/Sm*A* transition the narrow line from the isotropic phase disappears decisively at 118 °C (see again Fig. 2). This may be treated as the transition temperature from the Iso to the Sm*A* phase. However, above the Iso/Sm*A* phase transition a weak doublet starts to arise at higher temperatures, even at 130 °C. This effect may indicate the formation of some ordered domains in the isotropic phase close to the Iso/Sm*A* phase transition. The coupling constant (C_{FH}) was determined from the doublet of NMR lines presented in Fig. 2. This constant equals the difference in the chemical shift of the doublet lines. In D16 the value of C_{FH} varies from 10.30 to 15.15 kHz and is defined mostly by the benzene ring geometry and by its chemical environment, which is constantly changing with temperature due to molecular ordering and molecular dynamics.

As can be seen in Fig. 3, all mesophases existing in D16 are reflected in the observed $C_{FH}(T)$ dependence. In the Iso/Sm*A* phase transition a small jump in the value of the coupling constant is observed. After the phase transition to Sm*A* phase, the value of C_{FH} gradually increases with decreasing temperature in the whole temperature range of this mesophase. This tendency continues up to 60 °C at which the Sm*A*/Sm$C_\alpha{}^*$ phase transition occurs. The constant C_{FH} slowly decreases with decreasing temperature in Sm$C_\alpha{}^*$ phase, but below the Sm$C_\alpha{}^*$/Sm$C_\beta{}^*$ phase transition at 50 °C essentially an increase in the $C_{FH}(T)$ dependence is observed again. At first, in Sm$C_\beta{}^*$ phase the increase is moderate, but when the temperature drops below 40 °C, the increase is steep. At 35 °C, a sudden change in C_{FH} was observed indicating the temperature region in which the crystallization process

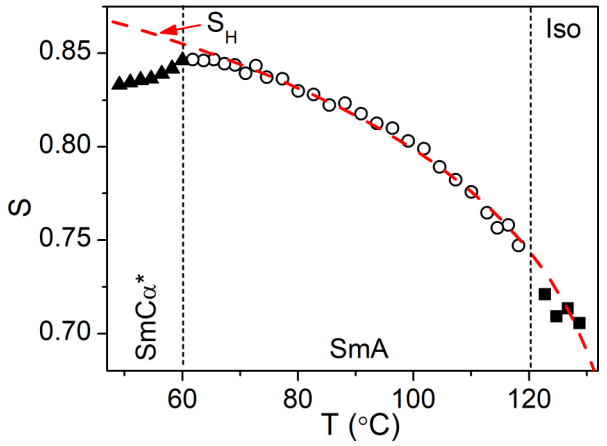

FIG. 4. The temperature dependence of the orientational order parameter, S, in the SmA phase and Sm$C_\alpha{}^*$ phase of D16 determined from the ^{19}F NMR measurements; the dashed line was obtained from the fit to the Haller equation.

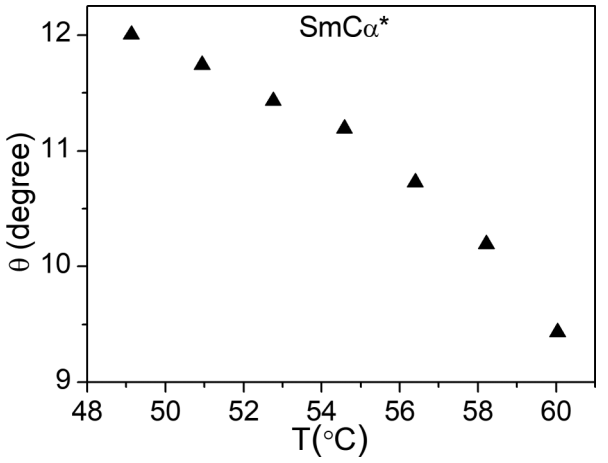

FIG. 5. Temperature dependence of the tilt angle θ in Sm$C_\alpha{}^*$ phase of D16 determined from the ^{19}F NMR measurements.

develops. At lower temperatures the coexistence of the Sm$C_\beta{}^*$ and crystal phase was manifested. The intensity of the double line was quickly decreasing to its final disappearance at 23 °C at which the sample completely crystallized.

The ^{19}F NMR spectroscopic results presented above are fully consistent with our previous results obtained with dielectric spectroscopy [15] and differential scanning calorimetry (DSC) (see the Supplemental Material [23] Fig. S1). Although the presented measurements were performed at a high magnetic field (11.74 T), no influence on the orientational order of the LC molecules by forcing them to align with their long axes along the external magnetic field was detected, and it was possible to determine the temperatures of all phase transitions in D16 [28].

The data presented in Fig. 3 for the SmA and Iso phases were analyzed using the Haller function [29,30]:

$$S(T) \propto C_{FH} = A(1 - T/T_{IS})^{\gamma}, \tag{1}$$

with the following parameters: $A = (13.8 \pm 0.2)$ kHz, $T_{\rm IS} = (411 \pm 2)$K, $\gamma = 0.096 \pm 0.010$ (see the Supplemental Material [23] Fig. S2). As a result the temperature dependences of the orientational order parameter, $S(T)$, in the Iso, SmA, and Sm$C_\alpha{}^*$ phases were obtained (Fig. 4).

On cooling the sample in a magnetic field of 11.74 T the order parameter S increases with temperature in the Iso and SmA phases (squares in Fig. 4), whereas in Sm$C_\alpha{}^*$ the value of S decreases (triangles) as a consequence of the formation of a helicoidal structure. In contrast to the SmA phase in the Sm$C_\alpha{}^*$ phase a nonzero tilt angle θ increases on cooling the sample from 9.4 degrees at 60 °C up to 12.0 degrees at 50 °C (Fig. 5). The small values of θ observed are characteristic for the Sm$C_\alpha{}^*$ phase [11,31]. The tilt angles in Sm$C_\alpha{}^*$ were estimated based on the expression

$$\theta = \arccos\left[2/3\,(S^H/S + 1)\right]^{1/2}, \tag{2}$$

where S is the order parameter in Sm$C_\alpha{}^*$ and S^H is the order parameter extrapolated from SmA to Sm$C_\alpha{}^*$ using the Haller expression [32]. The determined values of S and θ were used in the NMR relaxometry analysis presented below.

As can be seen the ^{1}H spectra are more complex in comparison with the ^{19}F ones. This indicates a high potential of this sensitive and selective spectroscopy for determination of important physical properties of LCs including molecular order in different phases. Figure 6 presents the proton spectra obtained as a function of temperature.

B. ^{19}F NMR diffusometry

The ^{1}H NMR diffusion measurements were performed in the isotropic phase of D16. Figure 7 shows the results obtained at 125 °C. The NMR spin echo signal attenuation measured as a function of a magnetic field gradient (g) was caused by the random translational movement of the LC molecules within the so-called diffusion time (Δ).

The observed signal intensities, $E(g)$, are described by

$$E(g) = E_0 \exp\left[-\gamma^2\delta^2 g^2 D\left(\Delta - \frac{\delta}{3}\right)\right], \tag{3}$$

where E_0 is the echo amplitude without the magnetic field gradient applied, γ is the gyromagnetic ratio, δ is the length of the gradient pulses, and D is the self-diffusion coefficient. During the measurements at 125 °C, the gradient value was varied in 22 steps from 0 to 0.06 T/m. The δ and Δ

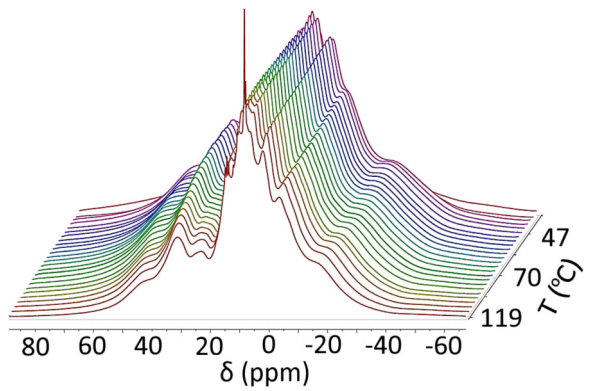

FIG. 6. ^{1}H NMR spectra recorded as a function of temperature in D16 at a magnetic field of 11.74 T, $\delta-$ chemical shift.

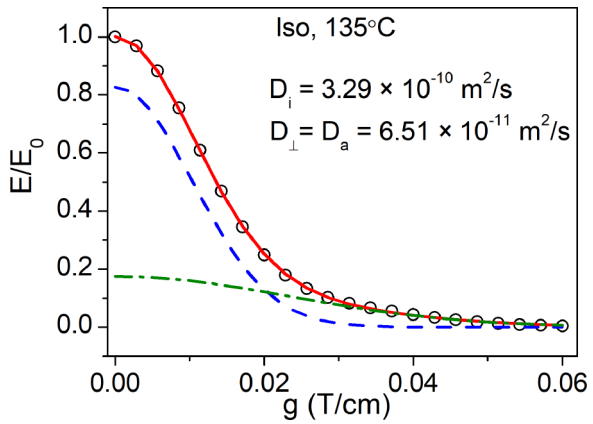

FIG. 7. Normalized experimental spin echo signal attenuation as a function of magnetic field gradient and model fitting curves observed in the isotropic phase of D16 at 135 °C as explained in the text. D_i and D_a, denote the molecular diffusion constants, respectively, for the isotropic process occurring outside the clusters (dash blue curve) and the anisotropic one associated with the molecules within the clusters (dash-dot green curve). The solid red line is the best fit of the biexponential Eq. (3) to the experimental points (circles).

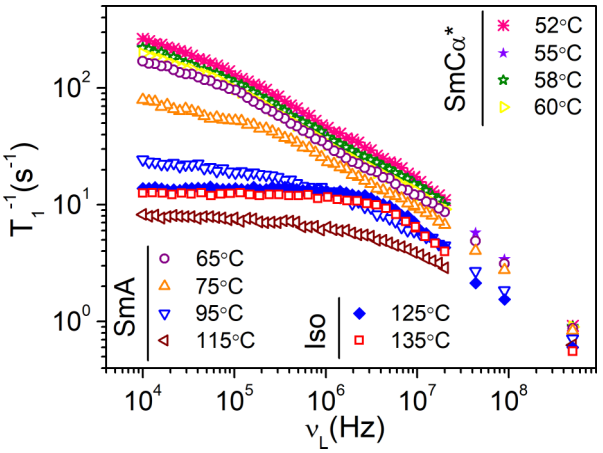

FIG. 8. The relaxation dispersion profiles of proton spin-lattice relaxation rate $1/T_1$ in D16 at various temperatures including three different LC phases.

parameters were kept constant during the experiments and were equal to 1 ms and 20 ms, respectively.

In Fig. 7 the experimental diffusion data collected in the isotropic phase of D16 at 135 °C are presented in the form of Gaussian decay profiles. The normalized echo integral amplitudes are plotted against gradient strengths (the data for 125 °C are presented in Supplemental Material [23], Fig. S3). The solid line represent the best fits of Eq. (3) to the experimental points. As shown, the decay profile is biexponential, and only two-component fits give satisfactory results. Therefore two diffusion constants, D_i and D_a, were obtained, respectively, for the isotropic molecular diffusion outside the clusters (blue curve in Fig. 7) and the anisotropic diffusion inside the clusters (green curve in Fig. 7). These diffusion results can be explained assuming that the LC molecules are partially ordered in clusters, even 17 °C above the Iso/Sm*A* transition. This assumption is in agreement with the results obtained from the ^{19}F NMR spectroscopy discussed before.

The presence of the molecular clusters in the isotropic phase in some LCs was previously described in Refs. [18,33–37]. For instance, Panarin *et al.* confirmed the existence of the cybotatic clusters of molecules at a temperature close to 2–3 °C above the isotropic/cybotactic nematic (Iso/N_{cybC}) transition [33]. In the cybotactic LC system (BCN66) the clusters in the Iso and N_{cybC} phases show ordering close to the Sm*C* type; however, it was formed by a much smaller fraction of molecules than that observed by us in the Iso phase in D16. At temperature corresponding to the Iso/N_{cybC} transition this fraction of molecules does not exceed 0.2%, whereas in D16, even 17 °C above the Iso/Sm*A* transition, approximately 20% of the LC molecules are associated with the clusters. The number of molecules involved in clusters in the N_{cybC} phase is increasing when decreasing the temperature. In D16 the fraction of molecules organized in clusters was assessed from diffusion contributions identified by the PFG NMR technique in the isotropic phase (Fig. 7).

For the cybotactic groups of molecules in the isotropic phase the layered structure of the smectic-type phase was also found in an alkylcyanobiphenyl (nCB) family of LCs. In these compounds for $n = 10$, 11, 12, and 14 the direct Iso/Sm*A* phase transition was observed [34]. The pretransitional effect in the isotropic phase of nCB was studied with light scattering [35], high-resolution calorimetry [36], and also in 10CB and 11CB with FFC NMR relaxometry [37]. In contrast to D16 the *n*CB materials are characterized by simple chemical structure and do not exhibit antiferroelectric phases. 10CB, 11CB, 12CB, and 13CB show only one LC phase (Sm*A*).

C. ^{1}H NMR relaxometry

The proton spin-lattice relaxation times (T_1) presented as relaxation rates ($1/T_1$) were measured as a function of the magnetic field strength. Figure 8 presents the relaxation dispersion profiles (NMRD) recorded for D16 as a function of temperature in the external magnetic field, B, in the range from 0.235 mT to 11.74 T. In the figure the magnetic field is expressed in the frequency units, according to the relation $\nu_L = \gamma B/(2\pi)$, where γ is the gyromagnetic ratio.

In the isotropic phase at 135 and 125 °C (results presented in Fig. 8 as squares and diamonds, respectively) the spin-lattice relaxation rate ($1/T_1$) below 10 MHz is higher than that measured at 115 °C in the Sm*A* phase (triangles-left). Figure 9 shows the $1/T_1$ values as a function of temperature. The data were obtained at selected low and high Larmor frequencies (i.e., 10 and 500 MHz).

As can be seen, the Iso/Sm*A* phase transition detected on cooling the sample at 10 kHz is marked by an apparent jump of the relaxation time T_1, in contrast to the almost flat dependence observed at 500 MHz. In turn, for SmC_α* phase (below 60 °C) a change in the $1/T_1$ slope is visible relative to that observed at 10 kHz in Sm*A* phase, whereas the effect is negligible for the dependence detected at 500 MHz. The above results indicate that the relaxation measurements performed at low magnetic field are especially important when dynamical properties of the phase SmC_α* are carefully investigated.

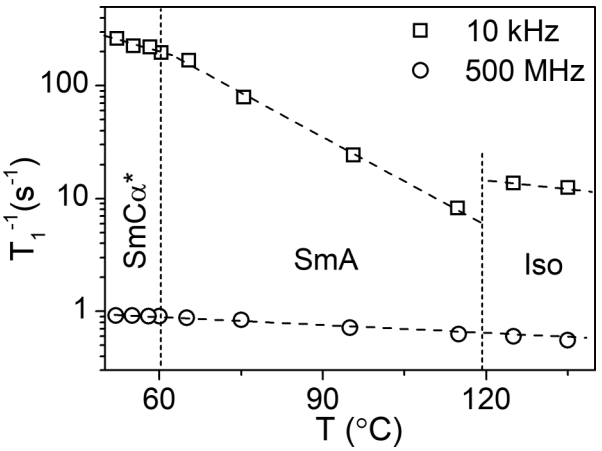

FIG. 9. Temperature dependence of $1/T_1$ at Larmor frequency 10 kHz and 500 MHz in the isotropic, Sm*A*, and Sm$C_\alpha{}^*$ phases of D16. The dashed lines are a guide to the eye.

Molecular motions influence the ^{1}H spin-lattice relaxation. The molecular motions induce fluctuations of the proton-proton dipolar interactions, thus affecting the magnetic NMR relaxation rates. Due to this fact it is possible to characterize the movements of molecules through the analysis of the NMRD profiles ($(1/T_1)$ (ν_L, T)). The total spin-lattice relaxation can be expressed as a sum of individual contributions related to a different type of molecular processes occurring at their characteristic timescales. Each contribution to the relaxation is analyzed in terms of an appropriate theoretical model. In D16, we considered both local (rotations and self-diffusion) and collective molecular motions (layer undulations, tilt direction fluctuations, order parameter fluctuations).

Taking into account that in isotropic phase of D16 we found two diffusion processes described by the two diffusion coefficients, and that in this phase some orientational order was determined using ^{19}F spectroscopy, we assumed that the rearrangement of LC molecules in the isotropic phase in D16 can be schematically illustrated as in Fig. 10. The molecular system, consisting of the molecules inside and outside the clusters, was considered by us in further analysis of the relaxation profiles.

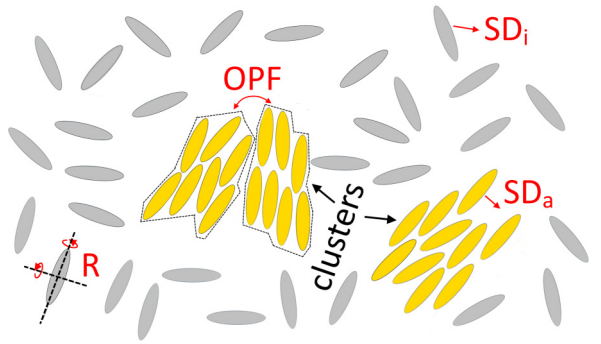

FIG. 10. Schematic illustration of different molecular motions in the system under investigation in the isotropic phase (R−rotations or reorientations, SD_a, SD_i−anisotropiclike and isotropic translational self-diffusions inside and outside the clusters, respectively; OPF−order parameter fluctuations) in the isotropic phase of D16.

Regardless of the phase analyzed (Iso, Sm*A*, Sm$C_\alpha{}^*$), two main relaxation processes were considered in the study, i.e., the molecular rotations or reorientations (R) and the translational self-diffusion (SD). The rotations or reorientations of molecules were described by the Nordio model [38]. It describes rotations of anisometric (rodlike) molecules around the long (z) molecular axis and the short one (x) and is given by Eq. (5)–(7).

With respect to the spin-lattice relaxation contribution by local molecular rotations/ reorientations (R) around the long (z) and short (x) molecular axes, the relaxation rate is given by the Nordio model [24]:

$$\left(\frac{1}{T_1}\right)_R = \frac{3}{4}K_D\left[J_R^{(1)}(\omega_L) + J_R^{(2)}(2\omega_L)\right], \tag{4}$$

where $\omega_L = 2\pi\nu_L$ and

$$K_D = \frac{3}{2}\left(\frac{\mu_0\gamma^2\hbar}{4\pi}\right)^2, \tag{5}$$

is the dipolar coupling constant, and the spectral density function, $J_R{}^{(k)}$ (for $k = 1, 2$) is written as

$$J_R^{(k)} = \frac{4}{3}(k)^2\sum_{m=0}^{2}\frac{\overline{\left|d_{m,0}^2(\alpha_{ij})\right|^2}}{r_{ij}^6} \times c(k,\ m)\frac{\left(\tau_{k,\ m}^2\right)^{-1}}{k^2\omega_0^2 + \left(\tau_{k,\ m}^2\right)^{-2}}, \tag{6}$$

where $\tau_{k,m}{}^2$ depends on correlation times for rotations around a short (τ_x) and long molecular axis (τ_z):

$$\left(\tau_{k,\ m}^2\right)^{-1} = \tau_z\left[\frac{1}{\beta_{k,m}^2} + \left(\frac{\tau_x}{\tau_z} - 1\right)m^2\right]. \tag{7}$$

In Eqs. (6) and (7), $c(k,m)$ and $\beta_{k,m}^2$ are numerical functions, and $d_{m,0}^2(\alpha_{ij})$ are the reduced Winger matrices [39] [Supplemental Material [23] Eq. (S5)].

The translational self-diffusions of molecules inside (SD_a) and outside the clusters (SD_i) were considered separately. The translational diffusion outside the clusters was described in terms of the theoretical model proposed by Torrey, Eq. (8), whereas the diffusion inside the clusters was considered using the model described by Žumer and Vilfan, Eq. (9). To fully reproduce the NMRD profiles in the whole frequency range studied, besides the $(1/T_1)_R$ and $(1/T_1)_{SD}$ contributions, an additional mechanism of the relaxation referring to the order parameter fluctuations (OPFs) was taken into account, Eq. (10).

The Torrey's model associated with the translational self-diffusion for isotropiclike system can be written in the form [25,40]

$$\left(\frac{1}{T_1}\right)_{SD_i} = \frac{9}{8}\gamma^4\hbar^2\left(\frac{\mu_0}{4\pi}\right)^2\frac{n\tau_D}{d^3} \times \left[\mathcal{T}(\alpha, \omega\tau_D) + 4\mathcal{T}(\alpha, 2\omega\tau_D)\right], \tag{8}$$

where d is the closest distance between the molecules, τ_D is the average time between molecular translational jumps $n - {}^1$H spin density, $\alpha = \langle a^2\rangle/12d^2$, and $\langle a^2\rangle = 6\tau_D D_i$ is the mean-square root of the molecular jump distance, D_i is

the diffusion constant, and $\mathcal{T}(\alpha, x)$ are analytical functions [25,40].

For the Sm*A* phase, the numerical function proposed by Torrey was expanded by Žumer and Vilfan, who took into account the anisotropy of the system. As a result, the following expression for the spin-lattice relaxation contribution related to self-diffusion was considered [41–43]:

$$\left(\frac{1}{T_1}\right)_{SD_a} = \frac{3}{4} K_D \frac{n\tau_{D_\perp}}{d^3} \times Q\left(\omega_L \tau_{D_\perp}, \frac{a_\perp^2}{d^2}, \frac{l}{d}, \frac{D_\parallel}{D_\perp}\right), \quad (9)$$

where $\langle a_\perp^2 \rangle = 4\tau_{D_\perp} D_\perp$, d is the width of molecule, l is the layer thickness, n is the spin density, $\tau_{D_\perp}$ is the mean square of molecular jump time, and $D_\perp$ and $D_\parallel$ are diffusion constants of molecules in two perpendicular directions with respect to the smectic layers normal; $Q(\omega_L \tau_{D_\perp}, \langle r_\perp^2 \rangle / d^2)$ is a dimensionless function calculated numerically [26].

OPFs have been reported in literature in association with nematiclike order of molecules encountered in small domains in the isotropic phase, close to the isotropic or nematic transition [43]. The OPF process detected in the isotropic phase is also classified as a type of collective motion.

The OPF relaxation contribution can be described by the following expression [40]:

$$\left(\frac{1}{T_1}\right)_{\mathrm{OPF}} = \frac{A_{\mathrm{OPF}}}{\omega_L^{1/2}} \int_0^{\nu_{\mathrm{cM}}^{\mathrm{OPF}}/\nu_L} \frac{\sqrt{x}}{1 + \left(x + \nu_0^{\mathrm{OPF}}/\nu_L\right)^2} \, dx, \quad (10)$$

where A_{OPF}, $\nu_{\mathrm{cM}}^{\mathrm{OPF}}$, and ν_0^{OPF} depend on viscoelastic parameters in the isotropic phase and denote, respectively, the strength of the OPF process and the high and low cut-off frequency.

In contrast to the isotropic phase, in the smectic phases of D16 two types of collective fluctuations related to layer undulations (LUs) and tilt direction fluctuations (TDFs) can observed. The presence of these collective fluctuations is a feature of molecular dynamics in LC ordered phases formed by LC molecules.

The model of the NMR relaxation corresponding to the LU and TDF motions can be expressed by the general formula [18]

$$\left(\frac{1}{T_1}\right)_{\mathrm{CM}} = \frac{A_{\mathrm{CM}_k}}{2\pi \nu_L^k} \left[f_k^{\mathrm{CM}}\left(\frac{\nu_{\mathrm{cM}}^{\mathrm{CM}}}{\nu_L}\right) - f_k^{\mathrm{CM}}\left(\frac{\nu_{\mathrm{cm}}^{\mathrm{CM}}}{\nu_L}\right) \right], \quad (11)$$

where $k = 1/2$ or $k = 1$ depending on the TDF or LU process, respectively, $f_k^{\mathrm{CM}}(x)$ are cut-off functions [see the Supplemental Material [23] Eq. (S7)]. A_{CM_k}, $\nu_{\mathrm{cM}}^{\mathrm{CM}}$, and $\nu_{\mathrm{cm}}^{\mathrm{CM}}$ are the strengths of collective motions and the high and low cut-off frequencies, respectively [see the Supplemental Material [23] Eqs. (S8)–(S11)]. These values depend on viscoelastic properties of the sample, the size of the LC molecule, and the correlation length of the collective fluctuations [42,18].

At low frequencies, $\nu_L < \nu_{\mathrm{cm}}^{\mathrm{CM}}$,$J(\nu_{\mathrm{L}})$ tends to a constant, whereas in the range of $\nu_{\mathrm{cm}}^{\mathrm{CM}} < \nu_L < \nu_{\mathrm{cM}}^{\mathrm{CM}}$, the slope of $J(\nu_L)$ is proportional to ${\nu_L}^{-1/2}$ for the TDF process and $J(\nu_L) \propto {\nu_L}^{-1}$ for the LU process (see the Supplemental Material [23] Fig. S4) [44].

All molecular processes described above and involved in the spin-lattice relaxation in smectic phases are schematically illustrated in Fig. 11.

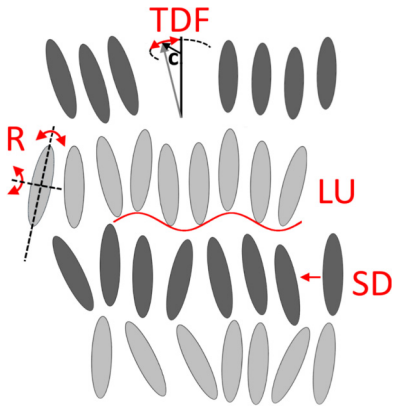

FIG. 11. Local (R−rotations or reorientations, SD−translational self-diffusion) and collective (LU−layer undulations, TDF−tilt direction fluctuations) molecular processes observed in the smectic phases of D16.

IV. SPIN-LATTICE RELAXATION ANALYSIS

All NMRD data were analyzed using the above theoretical models' contributions. The model fitting was made using the least square minimization method aiming at a global minimum provided by *fitteia* platform [40]. In order to achieve the best model fits to the experimental results it was necessary to consider the $1/T_1$ frequency dependence and the temperature dependence of the model fitting parameters.

For the isotropic phase (Fig. 10) the relaxation rate used was:

$$\left(\frac{1}{T_1}\right)_{\mathrm{Iso}} = 0.8\left(\frac{1}{T_1}\right)_{\mathrm{RD}_i} + 0.2\left(\frac{1}{T_1}\right)_{\mathrm{RD}_a} + 0.8\left(\frac{1}{T_1}\right)_{\mathrm{SD}_i} + 0.2\left(\frac{1}{T_1}\right)_{\mathrm{SD}_a} + 0.2\left(\frac{1}{T_1}\right)_{\mathrm{OPF}}. \quad (12)$$

In view of the results from diffusometry and ^{19}F spectroscopy, in the above expression two self-diffusion and rotation or reorientation contributions were considered. The factors 0.2 and 0.8 in Eq. (12) were calculated from the two diffusion contributions identified by PFG NMR technique in the isotropic phase of D16 (Fig. 7) in which approximately 20% of the LC molecules are associated with the clusters, and remaining 80% with disordered species.

The parameters assessed from the chemical structure of D16 and kept constant during the fitting procedure were the distance of the closest approach $d \cong 5 \times 10^{-10}$ m, the geometrical factors of $A_0 \cong 5.8 \times 10^{57}\,\mathrm{m}^{-6}$, $A_1 \cong 4.6 \times 10^{57}\,\mathrm{m}^{-6}$, $A_2 \cong 10 \times 10^{57}\,\mathrm{m}^{-6}$ (see the Supplemental Material [23] Eq.(S5)), and the proton density $n = 4.8 \times 10^{28}\,\mathrm{m}^{-3}$. Thus, for relaxation data analysis in the isotropic phase, only five free-fitting parameters (i.e., τ_x, τ_z, A^{OPF}, $\nu_{\mathrm{cM}}^{\mathrm{OPF}}$, and $\nu_{\mathrm{cm}}^{\mathrm{OPF}}$) were fitted to the experimental points using Eq. (12).

Figure 12 shows the NMRD profiles recorded for D16 LC in the isotropic phase at 125 °C. The black solid lines represent the best fit of Eq. (12) to the experimental points, and the dashed color lines show the individual contributions to the overall relaxation. As can be seen, the molecular rotational dynamics brings a contribution mainly in the highest frequency range (above 100 MHz), whereas the contribution

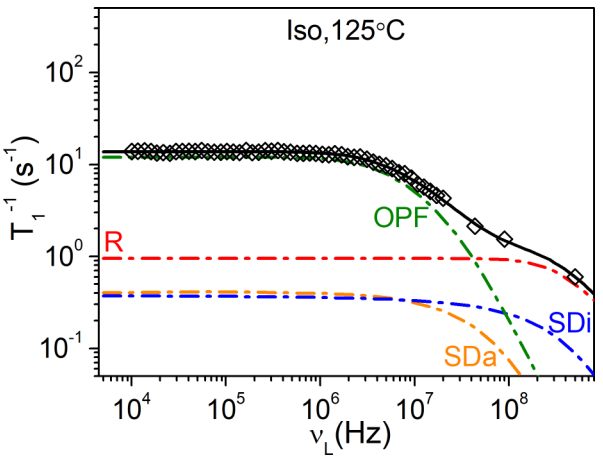

FIG. 12. Experimental data (symbols) and calculated model fitting curves (solid lines) obtained for the best model fit as explained in the text in the isotropic phase (Iso) of D16 at 125 °C; individual relaxation processes (dashed lines) are marked as molecular rotations or reorientations (R), translational self-diffusion inside SD_a and outside the clusters (SD_i), and order parameter fluctuations (OPF).

from the isotropiclike translational self-diffusion (SD_i) is less significant in this frequency region. In the frequency range between 4 and 100 MHz, the dynamical process related to the clusterlike (anisotropiclike) translational self-diffusion (SD_a) occurs. The dominant contribution to the overall relaxation at a low frequency range is associated with the OPF process. The dynamical collective molecular processes expected in the isotropic phase of D16 in the partially ordered system are schematically illustrated in Fig. 10. The parameters of the fit of Eq. (12) to the experimental points are presented in Table I.

The relaxation model used to describe the molecular dynamics in the smectic phases of D16 included the following contributions:

$$\left(\frac{1}{T_1}\right)_{\mathrm{Sm}} = \left(\frac{1}{T_1}\right)_{R} + \left(\frac{1}{T_1}\right)_{\mathrm{SD}_a} + \left(\frac{1}{T_1}\right)_{\mathrm{LU}}, \tag{13}$$

$$\left(\frac{1}{T_1}\right)_{\mathrm{Sm}} = \left(\frac{1}{T_1}\right)_{R} + \left(\frac{1}{T_1}\right)_{\mathrm{SD}_a} + \left(\frac{1}{T_1}\right)_{\mathrm{LU}} + \left(\frac{1}{T_1}\right)_{\mathrm{TDF}}. \tag{14}$$

The relaxation data analysis in Sm*A* phase was performed at 115, 95, 75, and 65 °C. At 75 and 65 °C the model expressed by Eq. (13) did not work satisfactorily and the additional contribution TDF had to be included – Eq. (15). At low frequencies a strong deviation of T_1 dispersion from the

TABLE I. Fitting parameters in Eq. (12) to the experimental data at 125 °C (isotropic phase); $D_a = 4.90 \times 10^{-11}$ m^2/s, $D_i = 2.10 \times 10^{-10}$ m^2/s.

T(°C)	125
$A^{\mathrm{OPF}}(\times 10^5\ \mathrm{s}^{-3/2})$	2.1 ± 0.1
$\nu_{\mathrm{cm}}^{\mathrm{OPF}}(\times 10^6\ \mathrm{Hz})$	2.2 ± 0.1
$\nu_{\mathrm{cM}}^{\mathrm{OPF}}(\times 10^7\ \mathrm{Hz})$	3.3 ± 0.1
$\tau_z(\times 10^{-11}\ \mathrm{s})$	1.89 ± 0.1
$\tau_x(\times 10^{-9}\ \mathrm{s})$	1.2 ± 0.1

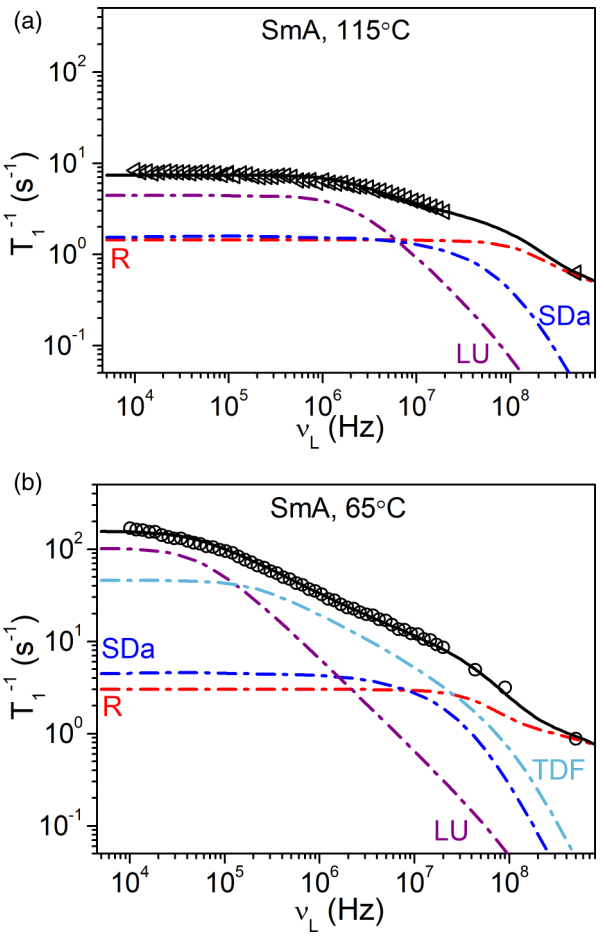

FIG. 13. Experimental data (symbols) and calculated model fitting curves (solid lines) obtained to the best model fit as explained in the text in the smectic-*A* phase (Sm*A*) of D16 at two temperatures: 115 °C (a), 65 °C (b); relaxation processes (dashed lines) are molecular rotations (R), translational self-diffusion (SD_a), layer undulations (LU), and tilt direction fluctuations (TDF).

characteristic frequency dependence of ν^{-1} was observed. In fact, taking into account the tilt of the molecules in the SmC_α* layers and the pretransitional effects observed in the isotropic phase, it is reasonable to assume the presence of domains composed of tilted molecules in the Sm*A* phase. Therefore, the analysis of the $1/T_1$ dispersions in the Sm*A* phase at 115 and 95 °C was performed using Eq. (13), whereas at 75 and 65 °C using Eq. (14); see Figs. 13(a) and 13(b), respectively. The additional TDF relaxation contribution required to obtain good fits in the Sm*A* phase at 75 and 65 °C is clear evidence of the onset of the of SmC_α* order. It is important to note that collective fluctuations of the tilt angle were previously observed in D16 using dielectric spectroscopy (see pp. 118–119 in Ref. [45]).

Figure 13 shows the NMRD profiles collected in the Sm*A* phase of D16 at 115 and 65 °C. The profiles at 115 and 65 °C were obtained close to the Iso/Sm*A* and Sm*A*/SmC_α* phase transition temperatures, respectively. As can be seen in the same figure, the R and SD_a processes are characterized by fast dynamics and contribute mainly to the NMR relaxation in the high frequency range ($\nu_L > 4 \times 10^7$ Hz), whereas the reverse

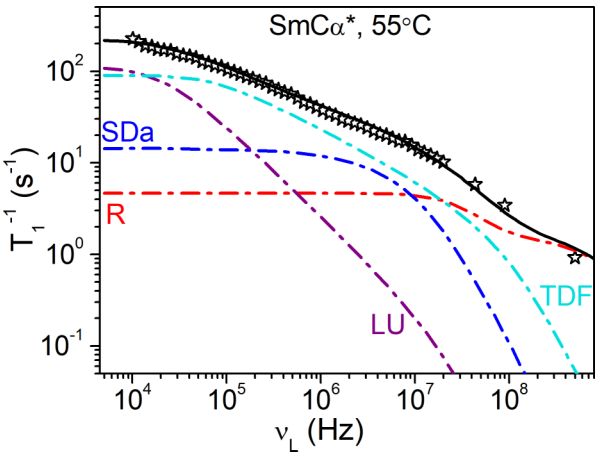

FIG. 14. Experimental data (symbols) and calculated model fitting curves (solid line) obtained for the best fit of the model as explained in the text in the SmC_α* phase of D16 at 55 °C; relaxation processes (dashed lines) are molecular rotations or reorientations (R), translational self-diffusion (SD_a), layer undulations (LU), and tilt direction fluctuations (TDF).

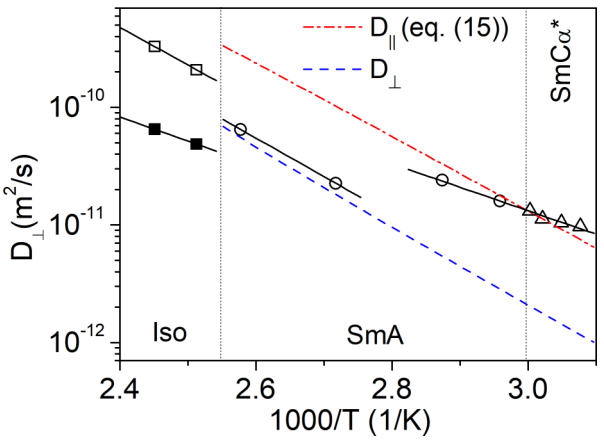

FIG. 15. Temperature dependence of the diffusion coefficient in the isotropic phase and principal diffusion coefficients in the LC state of D16; the self-diffusion values in smectic phases were obtained from the model fits; the red dot-dashed line and blue dashed line are calculated assuming the CM model [48]. For the group of points that fulfil the Arrhenius law (black solid lines) the fitting parameters are presented in the Supplemental Material [23] Eq. (S14).

is true for the LU processes. The LUs are characterized by the slow collective dynamics, and their significant contribution to the NMR relaxation is provided in the low-frequency range. In contrast to the rotations of the molecules, their self-diffusion, and the layer undulations, the tilt direction fluctuations contribute to the NMR relaxation mainly in the intermediate frequency range.

The results of the NMRD data analysis in the Sm*A* phase in D16 are similar to those obtained in a de Vries-type smectic-*A* (Sm A^*) phase in 9HL [18]. Gradišek *et al.* assumed that in the Sm A^* phase the molecular clusters are formed by molecules sharing the same tilt and azimuthal angles. In Sm A^* the azimuthal angles of the molecules are uncorrelated within the smectic layers, whereas in SmC_a^* a strong correlation takes place. Nevertheless, in both cases, it is reasonable to assume that in these mesophases the molecules fluctuate according to the TDF manner.

For all temperatures in the SmC_α^* phase Eq. (14) was applied to describe the experimental data (Fig. 14). In contrast to Sm*A* in the SmC_α^* phase we identified four dynamic processes occurring in the whole temperature range of this phase: R and SD_a (local dynamical processes) as well as LU and TDF (collective processes). The contributions to the NMR relaxation derived from these processes are presented in Fig. 14.

Equations (13) and (14) were fitted to the experimental data taking into account five free-fitting parameters: τ_x, τ_z, A^{LU}, ν_{cM}^{LU}, ν_{cm}^{LU}, A^{TDF}, ν_{cM}^{TDF}, ν_{cm}^{TDF}, and $D_\perp$.The fitting parameters in Eqs. (13) and (14) obtained for the best fit to experimental data in both Sm*A* and SmC_α^* phases are presented in Fig. 15 –Fig. 18 and in Table II (see also the Supplemental Material [23] Tables S3 and S4).

When we compare the SmC_a^* phase with the antiferroelectic smectic-C_A^* (SmC_A^*) phase formed by two helical superstructures, it can be concluded that in both phases the rotations or reorientations, self-diffusion, and layer undulations contribute to the spin-lattice relaxation. Furthermore, in the SmC_A^* phase the antiphase azimuthal angle fluctuations occur, whereas in the SmC_a^* phase the tilt direction fluctuations bring a significant contribution to the relaxation [46].

In the SmC^* phase the spin-lattice relaxation can be determined by the rotations or reorientations, self-diffusion and layer undulation [42], and sometimes the tilt direction fluctuations [19]. The same dynamic processes are taken under consideration in analysis of the NMRD data in the SmC_a^* phase. In the SmC_a^* phase the TDF process gives a major contribution to the spin-lattice relaxation in a broad range of Larmor frequencies, i.e., the amplitude A^{TDF} is higher and cut-off frequency ν_{cm}^{TDF} is lower than that in SmC^* in other chiral materials [18,19]. We can reasonably assume that in SmC_a^* the number of LC molecules fluctuating in the TDF manner is larger than in SmC^*, taking into account the fact that the low cut-off frequency of TDF is lower in the SmC_a^* than that observed for other SmC^* phases [18]. Moreover, the value of the helical pitch in SmC_a^* smaller than in the SmC^* phase reflects a higher degree of structural order, which

TABLE II. Fitting parameters for the models expressed by Eqs. (13) and (14) to the experimental data collected at 115, 65, and 55 °C.

LC phase	Sm*A*	Sm*A*	SmC_α^*
T (°C)	115	65	55
$D_\perp$ ($\times 10^{-11}$ m^2/s)	6.5 ± 0.2	2.3 ± 0.1	1.3 ± 0.1
θ (degrees)	0	0	11
A^{LU} ($\times 10^6$ s^{-2})	10.5 ± 0.1	6.6 ± 0.1	2.4 ± 0.1
ν_{cm}^{LU} ($\times 10^4$ Hz)	151.0 ± 0.2	4.1 ± 0.1	1.5 ± 0.1
A^{TDF} ($\times 10^4$ s$^{-3/2}$)	–	2.1 ± 0.1	2.6 ± 0.1
ν_{cm}^{TDF} ($\times 10^4$ Hz)	–	16.5 ± 1.3	6.2 ± 0.4
τ_z ($\times 10^{-10}$ s)	84.0 ± 4.2	1.6 ± 0.1	2.0 ± 0.1
τ_x ($\times 10^{-8}$ s)	84.7 ± 4.2	3.8 ± 0.2	6.8 ± 0.3

influences the viscoelastic properties of the phases [47] and the amplitude collective motions that becomes seemingly more important for TDF than for layer undulations. Nevertheless, the search for unique features of the SmC_a* phase determines the need for conducting further investigations.

V. TEMPERATURE DEPENDENCIES OF FITTING PARAMETERS

The values of the translational self-diffusion coefficient, $D_\perp$, corresponding to the best model fits to the experimental relaxation dispersion results are presented in Fig. 15 (all points). The self-diffusion coefficients in the isotropic phase were obtained from the pulsed field gradient (PFG) NMR measurements (squares). The self-diffusion constants in the smectic phases (circles and triangles) were obtained from the model data fits. The best model fits obtained at each temperature produced diffusion coefficients that do not fall into a single Arrhenius temperature dependence behavior [see the Supplemental Material [23] Eq. (S14)]. In the Sm*A* phase the behavior differs in two temperature ranges. At 115 and 95 °C (open circles) the self-diffusion coefficient estimated from the $1/T_1$ dispersion fits was close to that found for the Sm*A* clusters in the isotropic phase (full squares). At 75 and 65 °C (open circles) and for all temperatures in SmC_α* (triangles), different behavior of $D_\perp$ is presented in Fig. 15.

Moreover, the values of $D_\perp$ and $D_\parallel$ in the Sm*A* and SmC_α* phases were theoretically estimated applying Chu and Moroi (CM) model. The results are also presented in Fig. 15. The values of $D_\perp$ and $D_\parallel$ in the smectic phases in D16 are represented as dash and dash-dot lines, respectively. It was not possible to determine the diffusion coefficients directly from the diffusion experiment in the LC phases due to fast decay of the FID signal relative to the duration of the gradient pulses.

The CM model relates the diffusion constant in the isotropic phase (D_i) with the principal components of the diffusion tensor perpendicular ($D_\perp$) and parallel ($D_\parallel$) to the LC phase director expressed by the relations [48]

$$\begin{aligned} D_\parallel &= D_i[1 + 2S(1-\varrho)/(2\varrho+1)], \\ D_\perp &= D_i[1 - S(1-\varrho)/(2\varrho+1)], \end{aligned} \tag{15}$$

where $\rho = \pi d/4l$, and d and l are the diameter and length of the D16 molecule, respectively. The S and D_i were obtained from NMR spectroscopy and diffusiometry measurements, respectively (see Figs. 4 and 7).

From comparison the theoretically estimated values of $D_\perp$ (dash blue line) and those obtained as a result of the relaxation profiles' analysis in Sm*A* (open circles), one can indicate that only the diffusion values at 115 and 95 °C are consistent.

Figure 16 presents the values of the low cut-off frequency, ν_{cm}^{CM} (points), for LU and TDF relaxation contributions, corresponding to the best model fits to the experimental relaxation dispersion results. The lines presented in this figure represent the best fit of empirical equations to the ν_{cm}^{CM} values [see the Supplemental Material [23] Eqs. (S15) and (S16)]. The value of ν_{cm}^{CM} depends on viscoelastic properties of the LC system, and it is associated via the correlation length with the maximum size of the LC domain in which the tilt direction fluctuations occur or with the maximum size of the domain in the direction perpendicular to the layer's normal in which

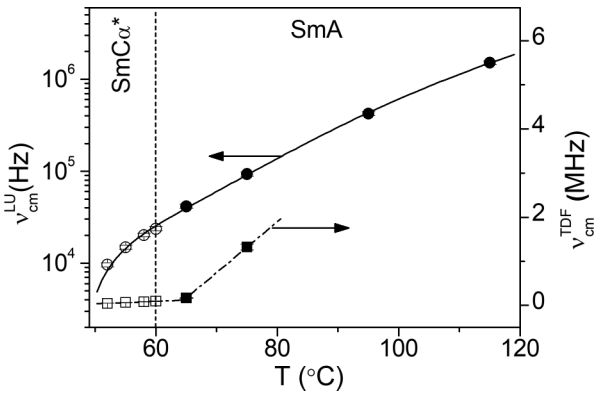

FIG. 16. Temperature dependencies of the low cut-off frequency of LU and TDF processes in the smectic phase of D16: values obtained from the model fits (points: ν_{cm}^{LU} – circles, ν_{cm}^{TDF} – squares), the best fits of empirical equations to the presented points (solid line); see the Supplemental Material [23] Eqs. (S15) and (S16).

layer undulations occur coherently [49]. The domain size is inversely proportional to the low cut-off frequency.

In general, the ν_{cm}^{CM} of LU and TDF decreases with decreasing temperature due to the fact that the effective viscosity of the material increases. The low cut-off of the LU process does not provide clear evidence of the phase transition between Sm*A* and SmC_α* phases. The low cut-off frequency associated with the TDF process shows a strong decrease by a factor of 10 close to the Sm*A*/SmC_α* transition temperature remaining almost constant for lower temperatures. It can be explained if one assumes that in Sm*A* the domains of SmC_α* are formed at temperatures even 15 °C above the Sm*A*/SmC_α* transition. The TDF process is related to the azimuthal fluctuations of the tilt direction. It is observed only in the sample regions in which the molecules are tilted. In D16 we observed the TDF process in Sm*A* even 15 °C above phase transition to SmC_α*. Due to the onset of the SmC_α* phase structure in D16, the size of domains increases on cooling the sample, and therefore the low cut-off frequency of TDF decreases with decreasing temperature. The ν_{cm}^{CM} value of TDF is smaller in the SmC_α* than in the Sm*A* phase because in the SmC_α* phase all molecules are tilted, and TDF fluctuations propagate in the sample over longer distances. The almost constant ν_{cm}^{CM} value of TDF in SmC_α* evidences smaller changes in the phase structure, or it is the result of the fact that viscoelastic constants characterizing SmC_α* depend less on the temperature in comparison with viscoelastic constants characterizing Sm*A*.

In Fig. 17 the amplitudes of LU and TDF motions, A_{CM} (points), correspond to the best model fits of Eq. (14) to the NMRD data. The lines represent the best fit of the empirical equations describing the temperature dependence of the strength of the layer undulations to the A_{CM} values [see the Supplemental Material [23] Eqs. (S17) and (S18)].

The amplitude A_{TDF} associated with layer undulations increases in the temperature range of Sm*A* and SmC_α* phases (dash-dot line), whereas A_{LU} associated with tilt direction fluctuations decreases as a function of temperature (dashed line). The linear fits for the A_{LU} parameter in Sm*A* and for A_{TDF} in SmC_α* show different slopes. Moreover, the

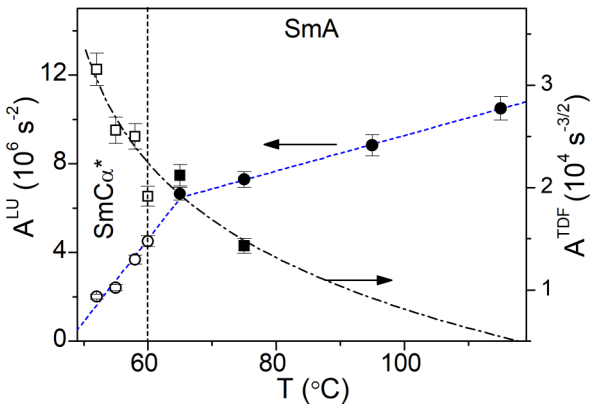

FIG. 17. Temperature dependencies of A^{LU} and A^{TDF} in the smectic phase in D16: values obtained from the model fits (points: A^{LU}−circles, A^{TDF}−squares), the best fits of empirical equations to the presented points (lines); see the Supplemental Material [23] Eqs. (S17) and (S18).

temperature dependence of A_{TDF} in the SmC_α* phase exhibits a faster increase than that observed in SmA.

Figure 18 presents the correlation times as a function of temperature for local molecular rotations corresponding to the best model fits to the $1/T_1(\nu_L)$ experimental dependencies. The solid lines are a guide for the eye. The R contribution to the relaxation is observed at the high frequencies at which rotations bring the dominant contribution to the overall relaxation of the system (Figs. 12 and 13). The correlation times τ_x and τ_z describe the rotations around the short and long molecular axis, respectively. As expected, the τ_z times are shorter than τ_x due to the smaller moment of inertia about the long molecular axis. The jump in the value of the correlation times observed on cooling at the Iso/SmA phase transition temperature is caused by an increase in the molecular order. A similar effect is observed at the SmC_α*/SmA phase transition for the correlation times associated with the rotations around the short molecular

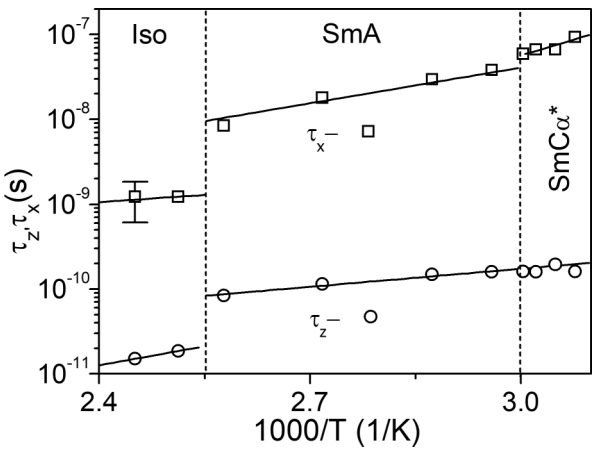

FIG. 18. Temperature dependencies of the correlation times of rotations around the short τ_x and long τ_z molecular axis in isotropic and smectic phases; solid line are fits made using the Arrhenius temperature dependencies; see the Supplemental Material [23] Eq. (S19) and Table S2.

axis. The value of τ_x in the SmA phase is smaller than that in SmC_α* as a consequence of molecular space restriction caused by layer shrinkage due to the tilt of the molecules.

VI. CONCLUSIONS

In this paper we have investigated the dynamics of the molecular processes in the antiferroelectric LC D16 using different NMR experimental techniques. Both ^{19}F NMR diffusometry and ^{19}F NMR spectroscopy have shown that in the isotropic phase of D16 at 125 °C and 135 °C a certain percentage of molecules form clusters with the SmA ordering. In fact, from the dipolar splitting of the ^{19}F NMR spectra some values of the order parameter were obtained. Also, from the pulsed field gradient measurements two diffusion coefficients were obtained for the two temperatures in this phase. The NMRD profiles in the isotropic phase were analyzed in terms of the three contributions coming from molecular rotations or reorientations, translational self-diffusion, and order parameter fluctuations in the molecular clusters. The contributions from the translational self-diffusion and rotations or rotations both inside and outside the clusters were considered separately.

The NMRD profiles in the SmA phase were fitted using rotations or reorientations, translational self-diffusion, and layer undulations. The values of the translational self-diffusion coefficients in the SmA phase obtained from the fits were compatible with those obtained for the isotropic phase. The values of the correlation times were compatible with those of the isotropic phase taking into account the difference in molecular order in the two phases. Close to SmA/SmC_α* phase transition the NMRD profiles could not be explained with just three relaxation contributions. A contribution with a $\omega^{-1/2}$ frequency dependence also had to be included, in view of the analysis of the NMRD profiles in the SmC_α* phase, in which fluctuations of the tilt direction were observed.

The fits obtained are self-consistent, which is evidenced by the temperature dependence of the fitting parameters. In fact, not only do the correlation times for rotations or reorientations evidence the Arrhenius temperature dependencies in SmA and SmC_α*, but also the self-diffusion coefficients in SmA obtained from the fits present the temperature dependence compatible with activation energies estimated from the data for the isotropic phase.

The collective motions are found to be sensitive to changes in the phase structure and molecular organization. The temperature dependences of the cut-off frequencies and the strength of the layer undulations and value of tilt direction fluctuations contributions are consistent with the changes in the phase structure and molecular arrangement in the smectic phases. In particular, the transition temperatures are obtained from the temperature dependence profiles of the fitting parameters. The fluctuations of the tilt direction observed for D16 here by NMR are compatible with the results obtained from our previous dielectric spectroscopy studies.

There are no conflicts to declare.

ACKNOWLEDGMENTS

The authors would like to acknowledge the financial support of the COST Action CA15209, "European Network on NMR Relaxometry," for Short Term Scientific Missions

(STSM) at the Instituto Superior Técnico in Lisbon, Portugal. The work was partially financed by the National Science Centre, Poland, within the grant MINIATURA 3, No. DEC-2019/03/X/ST5/01549.

[1] S. T. Lagerwall, *Ferroelectric and Antiferroelectric Liquid Crystals* (Wiley-VCH, New York, 1995).
[2] P. G. de Gennes and J. Prost, *The Physics of Liquid Crystals* (Oxford Science Publications, Oxford, 1995).
[3] S. Chandrasekhar, *Liquid Crystals* (Cambridge University Press, Cambridge, 1977).
[4] P. J. Collings and M. Hird, *Introduction to Liquid Crystals: Chemistry and Physics* (Taylor & Francis, London, 1997).
[5] J. P. F. Lagerwall and F. Gisselmann, in *Chiral Liquid Crystals*, edited by W. Kuczyński (Polish Academy of Sciences, Poznan, 2005), pp. 147–184.
[6] R. B. Meyer, L. Liébert, L. Strzelecki, and P. Keller, J. Phys. Lett. **36**, 69 (1975).
[7] D. M. Walba, *Advances in the Synthesis and Reactivity of Solids*, Vol. 1 (JAI Press Ltd., 1991), p.173.
[8] J. M. Oton, X. Quintana, P. L. Castillo, A. Lara, V. Urruchi, and N. Bennis, Opto-Electron. Rev. **12**, 263 (2004).
[9] X. Xun, D. J. Cho, and R. W. Cohn, Appl Opt. **45**, 3136 (2006).
[10] S. Kumari, M. B. Pandey, R. Bhar, I. M. L. Das, and R. Dabrowski, Phase Transit. **84**, 38 (2011).
[11] A. Labeeb, The rotational viscosity and field-induced transitions in the intermediate phases of ferroelectric liquid crystals, Ph.D. dissertation, University of Manchester, 2011.
[12] P. Mach, R. Pindak, A.-M. Levelut, P. Barois, H. T. Nguyen, H. Baltes, M. Hird, K. Toyne, A. Seed, J. W. Goodby, C. C. Huang, and L. Furenlid, Phys. Rev. E **60**, 6793 (1999).
[13] K. Nowicka, M. Knapkiewicz, N. Bielejewska, D. Dardas, W. Kuczyński, and J. Hoffmann, Liq. Cryst. **43**, 1778 (2016).
[14] J. P. F. Lagerwall, Phys. Rev. E **71**, 051703 (2005).
[15] M. Knapkiewicz, M. Sądej, W. Kuczyński, and A. Rachocki, Phys. Rev. E **96**, 052702 (2017).
[16] H. S. Chang, S. Jaradat, H. Gleeson, I. Dierking, and M. A. Osipow, Phys. Rev. E **79**, 061706 (2009).
[17] A. Labeeb, H. F. Gleeson, and T. Hegmann, Appl. Phys. Lett. **107**, 232903 (2015).
[18] A. Gradišek, V. Domenici, T. Apih, V. Novotná, and P. J. Sebastião, J. Phys. Chem. B **120**, 4706 (2016).
[19] A. Gradišek, T. Apih, V. Domenici, V. Novotna, and P. J. Sebastião, Soft Matter **9**, 10746 (2013).
[20] E. Carignani, L. Calucci, E. Juszyńska-Gałązka, M. Gałązka, M. Massalska-Arodź, C. Forte, and M. Geppi, J. Phys. Chem. B **120**, 5083 (2016).
[21] P. J. Sebastião, in *Field-cycling NMR Relaxometry: Instrumentation, Model Theories and Applications*, edited by R. Kimmich (Royal Society of Chemistry, London, 2018), pp. 255–302.
[22] V. Domenici, Liq. Cryst. Today **26**, 2 (2017).
[23] See Supplemental Material at http://link.aps.org/supplemental/10.1103/PhysRevE.101.052708 for details of the NMRD data analysis.
[24] P. L. Nordio and P. Busolin, J. Chem. Phys. **55**, 5485 (1971).
[25] H. C. Torrey, Phys. Rev. **92**, 962 (1953).
[26] M. Vilfan and S. Žumer, Phys. Rev. A **21**, 672 (1980).
[27] R. Y. Dong, *Nuclear Magnetic Resonance of Liquid Crystals* (Springer-Verlag, New York, 1997).
[28] F. Noack, Prog. Nucl. Magn. Reson. Spectrosc. **18**, 171 (1986).
[29] V. Domenici, A. Marini, C. A. Veracini, J. Zhang, and R. Y. Dong, ChemPhysChem **8**, 2575 (2007).
[30] M. Geppi, A. Marini, B. Mennucci, and P. Kula, Mol. Cryst. Liq. Cryst. **541**, 104 (2011).
[31] J. Hoffmann, F. Giesselmann, and W. Kuczyński, Phase Transit. **80**, 841 (2007).
[32] V. Domenici, M. Lelli, M. Cifelli, V. Hamplova, A. Marchetti, and C. A. Veracini, ChemPhysChem **15**, 1485 (2014).
[33] Y. P. Panarin, S. P. Sreenilayam, J. K. Vij, A. Lehmann, and C. Tschierske, Beilstein J. Nanotechnol. **9**, 1288 (2018).
[34] S. Urban, M. Massalska-Arodź, A. Würflinger, and R. Dąbrowski, Liq. Cryst. **30**, 313 (2003).
[35] H.. J. Coles and C. Strazielle, Mol. Cryst. Liq. Cryst. **49**, 259 (1979).
[36] G. Cordoyiannis, M. H. Godinho, C. Glorieux, and J. Thoen, Phase Transit. **82**, 280 (2009).
[37] F. Vaca Chávez, R. H. Acosta, and D. J. Pusiol, Chem. Phys. Lett. **392**, 403 (2004).
[38] R. Kimmich and E. Anoardo, Prog. Nucl. Magn. Reson. Spectrosc. **44**, 257 (2004).
[39] P. J. Sebastião, A. Gradišek, L. F. V. Pinto, T. Apih, M. H. Godinho, and M. Vilfan, J. Phys. Chem. B **115**, 14348 (2011).
[40] P. J. Sebastião, Eur. J. Phys. **35**, 015017 (2014).
[41] A. Carvalho, P. J. Sebastião, A. C. Ribeiro, H. T. Nguyen, and M. Vilfan, J. Chem. Phys. **115**, 10484 (2001).
[42] A. Ferraz, J. Zhang, P. J. Sebastião, A. C. Ribeiro, and R. Y. Dong, Magn. Reson. Chem. **52**, 546 (2014).
[43] R. Y. Dong, *Nuclear Magnetic Resonance Spectroscopy of Liquid Crystals* (World Scientific, Singapore, 2010).
[44] T. Apih, V. Domenici, A. Gradišek, V. Hamplová, M. Kaspar, P. J. Sebastião, and M. Vilfan, J. Phys. Chem. B **114**, 11993 (2010).
[45] M. Knapkiewicz, *Wpływ Sieci Polimerowej Na Właściwości Fizyczne i Dynamikę Molekularną Chiralnych Ciekłych Kryształów* (Institute of Molecular Physics, Polish Academy of Sciences, Poznan, Poland, 2020).
[46] A. Ferraz, A. C. Ribeiro, and H. T. Nguyen, Mol. Cryst. Liq. Cryst. **331**, 67 (1999).
[47] D. Dardas, Rheol. Acta **58**, 193 (2019).
[48] S. V. Dvinskikh, I. Furó, H. Zimmermann, and A. Maliniak, Phys. Rev. E **65**, 061701 (2002).
[49] A. Aluculesei, F. Vaca Chávez, F. Vaca, C. Cruz, P. J. Sebastião, N. G. Nagaveni, V. Prasad, and R. Y. Dong, J. Phys. Chem. B **116**, 9556 (2011).